

Chern Half metal: The Case of Graphene With Co or Rh Adatom

Jun Hu, Zhenyue Zhu and Ruqian Wu*

Department of Physics and Astronomy, University of California, Irvine, California 92697-4575, USA

The recent discovery of topological insulators—that act as insulators in their bulks yet possess quantized conducting edge or surface states—has triggered extremely active multidisciplinary research activities for the exploration of new fundamental science and exotic materials. One of the most interesting phenomena in this realm is the quantum anomalous Hall effect (QAHE). So far, the QAHE has been observed only in Cr-doped $(\text{Bi,Sb})_2\text{Te}_3$ yet at extremely low temperature. Therefore, it is important to search for new topological insulators with large topological band gap and high thermal stability for the realization of the QAHE. Here, we found a new class of topological insulator phase—Chern half metal which manifests the QAHE in the minority spin channel while is metallic in the majority spin channel—in Co or Rh deposited graphene, based on first-principles and tight-binding model calculations. Meanwhile, these systems have large perpendicular magnetic anisotropy energies of 5.3 and 11.5 meV, necessary for the observation of the QAHE and reasonably high temperature.

The search of new topological insulators that demonstrate the quantum anomalous Hall effect (QAHE) is a cutting-edge research topic in condensed matter physics and material science [1–8]. For the realization of the QAHE, the time-reversal symmetry (TRS) must be broken by using *intrinsic* magnetization rather than external magnetic field, through magnetic impurities [9, 10], adatoms [11, 12], or substrate [13]. Therefore, the realization of the QAHE in experiment is quite subtle. In addition, it is necessary to align the magnetization along the surface normal, in analog to the geometry of conventional anomalous Hall effect [14]. The only experimental observation of the QAHE was reported recently in Cr-doped $(\text{Bi,Sb})_2\text{Te}_3$ in an extreme experimental condition below 0.1 K [15], due to the tiny TI gap, and also complications in dealing with surfaces of three-dimensional TIs. Thus, searching for more feasible TIs especially in simple two-dimensional (2D) systems with large nontrivial band gaps is of great importance for the realization and exploitation of the QAHE.

It is known that the nontrivial band gaps in TIs are induced by the spin-orbit coupling (SOC) interactions. In addition, the *intrinsic* magnetization supplies an exchange field (M_{ex}) which splits the majority spin and minority spin electronic bands. Accordingly, there are two types of TI gaps for the QAHE, depending on the strength of M_{ex} , as presented by the schematic band structures in Fig. 1. The type-I band gap is produced by the interspin SOC interactions, i.e., between majority spin and minority spin states, when the M_{ex} is small. For large M_{ex} , the type-II band gaps are induced by the intraspin SOC interactions, i.e., between the states with same spin. The most studied magnetic TIs including the Cr-doped $(\text{Bi,Sb})_2\text{Te}_3$ [9–12, 15] have the type-I TI gaps, while the type-II TI gap was predicted in an organic material [16].

Note that both type-I and type-II TI gaps are global, and this condition has been believed to be necessary to give rise to the QAHE in previous studies. Interestingly, we can see another kind of SOC induced band gaps (denoted as type-III) in Fig. 1(b), that lead to a half metallic feature if the Fermi level (E_F) locates within them. The coupling between two spin channels around the type-III gaps are avoided, because different spin bands are separated in the Brillouin zone. We may expect that the type-III gaps also lead to the QAHE as the type-II TI gap

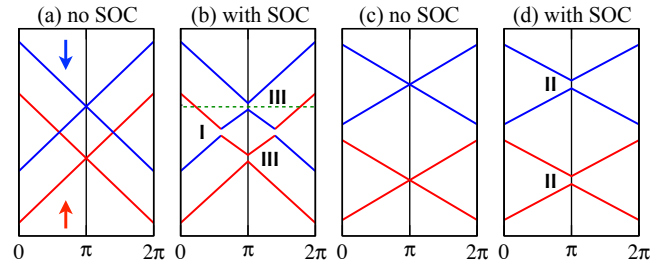


FIG. 1: **Schematic band structures for classifying the topological insulator gaps for QAHE.** (a) and (b) With small exchange field, (c) and (d) with strong exchange field. The red and blue arrows indicate the majority spin and minority spin states, respectively. Three types of SOC induced gaps are marked by ‘I’, ‘II’ and ‘III’. The type-III gap is distinguished from type-II gap because the other spin channel is metallic as indicated by the green dashed line in (b).

does. In this sense, materials with the type-III gaps become a new class of TIs for the realization and exploitation of the QAHE. Since the QAHE is characterized by nonzero integer Chern numbers [17, 18], we can call these materials *Chern half metals*.

Graphene can be a useful template to realize the QAHE in 2D systems at high temperature, due to its structural simplicity and stability. Huge TI gaps can be produced in graphene by heavy adatoms, taking advantage of the strong SOC on adatoms and the delocalization of graphene π bands which mediate the long-distance interactions between adatoms [19, 20]. The QAHE was indeed predicted in Fe [11] or W [12] deposited graphene, with type-I TI gaps of 5.5 or ~ 30 meV. The main drawback of these predictions is that both Fe/graphene and W/graphene prefer the in-plane spin orientation (see Fig. S1 and Ref. [12]), rather than as assumed to be perpendicular to the graphene plane as required by the QAHE. Here, we found that the Co/graphene and Rh/graphene have perpendicular easy axis with large magnetic anisotropy energies (MAEs) of 5.3 and 11.5 meV. Interestingly, they have type-III TI gap of 50 and 100 meV, respectively. We demonstrated that both gaps can give rise to the QAHE, based on the first-principles calculations and tight-binding (TB) model analyses. Therefore, the Co/graphene and Rh/graphene can be ex-

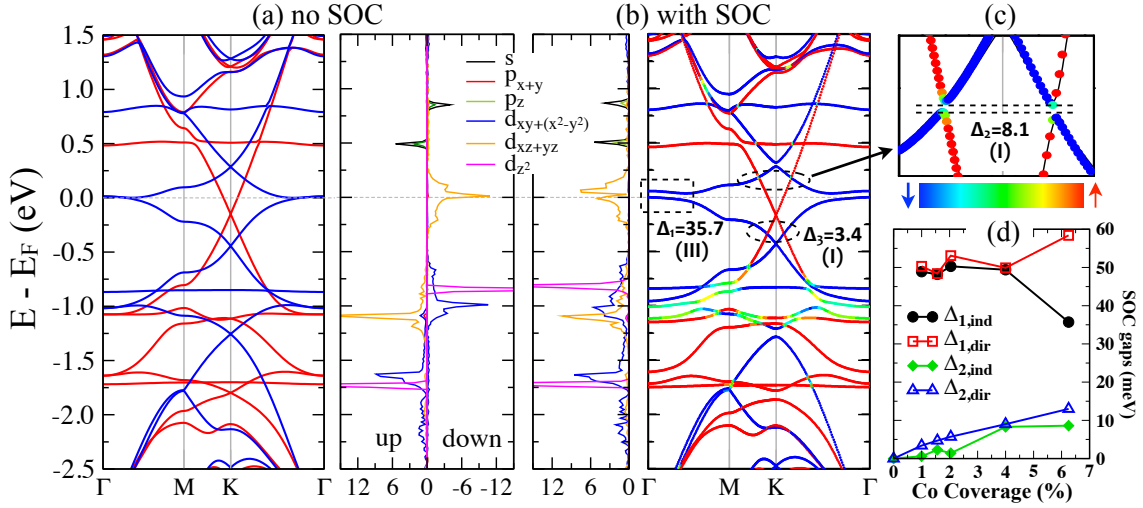


FIG. 2: **Electronic properties of a 4×4 graphene with one Co adatom.** (a) and (b) The spin-resolved band structures and projected density of states of Co-3d orbitals without and with SOC interactions. The Fermi level (E_F) is set as the zero energy, as indicated by the horizontal grey dashed line. The spin orientation of Co is set to perpendicular to the graphene plane. (c) Zooming in of the local band structure indicated by the arrow. The color bar indicates the relative ratio between the majority and minority spin states of the band structures. Three SOC induced gaps (Δ_1 , Δ_2 and Δ_3 given in meV) are specified in (b) and (c), with their classifications notated in the parentheses. (d) The Co coverage dependences of Δ_1 and Δ_2 . Here both the indirect and direct band gaps are plotted.

cellent Chern half metals which expand the topological insulator phase into half metals.

It has been shown that the d orbitals of transition metal adatoms on graphene strongly hybridize with graphene π bands, resulting in a series of impurity bands [11, 12, 20, 21]. Ding *et al* found that some 3d transition metal adatoms on graphene can generate type-I TI gaps, but these gaps are typically small and far away from the E_F [21]. To check whether the type-II and type-III TI gaps appear in graphene based systems, we carried out density functional theory (DFT) calculations to study the electronic and magnetic properties of all 3d transition metal adatoms on graphene. We found that they (except Ni) are spin-polarized and prefer the hollow site on graphene, in good agreement with previous calculations [21]. Their MAEs, calculated as $MAE = E(\rightarrow) - E(\uparrow)$ with the torque method [22–24], suggest that only Mn (MAE = +1.4 meV) and Co (MAE = +5.3 meV) on graphene have perpendicular spin orientation. The large positive MAE of Co/graphene provides high thermal stability of spin orientation and thus is good for the realization of QAHE if it does exist. From the band structures with the SOC involved in calculations, no type-II gap was found, because the exchange splitting of a single transition metal adatom is not large enough. Interestingly, we found a type-III gap in Co/graphene bands and the E_F locates right at its edge. This indicates the Co/graphene might be a Chern half metal. The origin and the topological feature of this gap thus deserve a special attention.

To reveal the evolution of the type-III gap of Co/graphene, let's first discuss the electronic properties without the involvement of the SOC. From the spin-resolved band structure and projected density of states (PDOS) in Fig. 2(a), we can see that the Co-3d orbitals are split into three groups: d_{z^2} , $d_{xz/yz}$,

and d_{xy/x^2-y^2} , due to the symmetry of the crystal field of graphene. The minority spin $d_{xz/yz}$ orbitals are nearly half occupied, and all the others are fully occupied, resulting in an electronic configuration of $d^9 s^0$ for the Co-3d orbitals and a spin moment of $\sim 1.0 \mu_B$. It should be pointed out that the adsorption position and electronic state of Co adatom on graphene is still in debate [25, 26], but it is commonly believed that the Co adatom is adsorbed on the hollow site of graphene with an electronic configuration of $d^9 s^0$ [21, 27], as found in our calculations.

Without SOC, the $d_{xz/yz}$ bands in the minority spin channel are degenerate near the E_F around the Γ point. Interestingly, a large type-III band gap (Δ_1) of 35.7 meV (or a direct band gap of ~ 58 meV) is produced by the intraspin SOC interactions between them, as shown in Fig. 2(b). Note that there is a tiny electron (hole) pocket in the majority (minority) spin channel, and the E_F is pinned at ~ 15 meV below the valence band maximum (VBM) of minority spin channel [see Fig. 3(a)]. Clearly, the Fermi level can be tuned easily into this gap by applying small positive gate voltage. Meanwhile, the majority spin states near the E_F show linear dispersion and are not much affected by the SOC interactions. As a result, the Co/graphene is a half metal when the E_F locates in the gap Δ_1 : conducting in the majority spin channel but insulating in the minority spin channel. From the matrix elements of the SOC Hamiltonian $\xi \mathbf{L} \cdot \mathbf{S}$, we found that the gap Δ_1 opens mainly because of the strong SOC effect through $\langle L_z \rangle = \langle d_{xz/yz}^o, \downarrow | L_z | d_{xz/yz}^u, \downarrow \rangle$. Here the superscripts o and u stand for the occupied and unoccupied status, respectively; and the arrow \downarrow indicates the minority spin. As $\langle L_{\pm} \rangle = \langle d_{xz/yz}^o, \downarrow | L_{\pm} | d_{xz/yz}^u, \downarrow \rangle = 0$, the gap Δ_1 disappears if the spin orientation is parallel to the graphene plane.

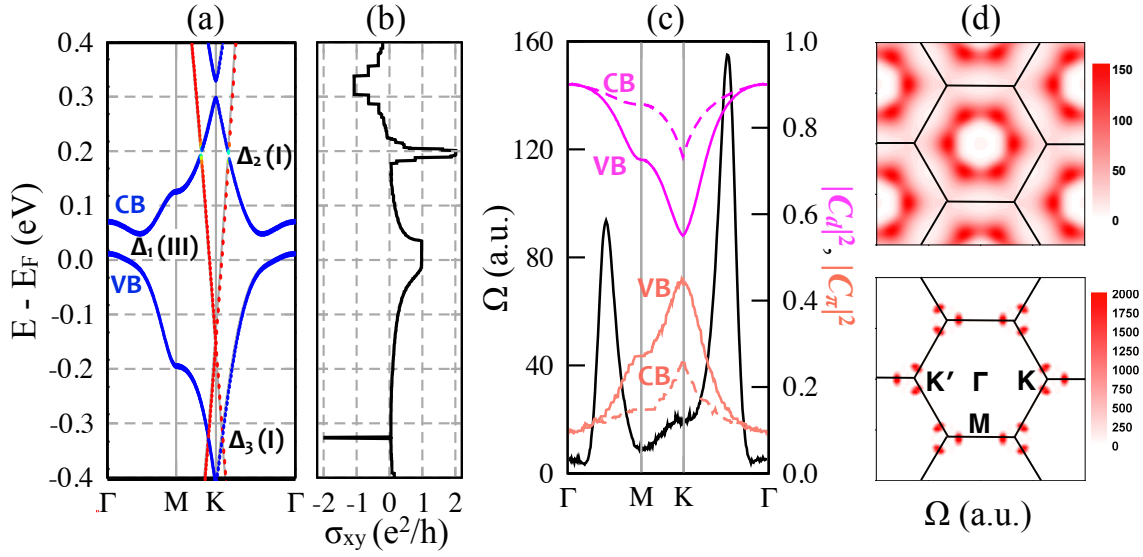


FIG. 3: **Band structure, anomalous Hall conductivity and Berry curvature.** (a) Band structure of Co/graphene with SOC. ‘VB’ and ‘CB’ denote the highest valence band and lowest contribution band in minority spin channel, respectively. The color scheme of the bands and the notations of the band gaps are the same as those in Fig. 2. (b) Fermi level-dependent anomalous Hall conductivity (σ_{xy}). (c) Berry curvature Ω (black curve) for the gap Δ_1 and weights of the Co $3d$ (magenta curves) and graphene π orbitals (salmon curves) for VB and CB. (d) Distribution of Berry curvature in the whole 2DBZ for Δ_1 (upper panel) and Δ_2 (lower panel).

Meanwhile, the magnetic anisotropy is the result of the competition between $\langle L_z \rangle$ and $\langle L_{\pm} \rangle$ [28, 29], so the large matrix element $\langle L_z \rangle$ is also the origin of the strong perpendicular magnetic anisotropy of Co/graphene. Since the gap Δ_1 mainly results from the SOC effect of Co adatoms, it’s instructive to see how it changes when the Co coverage decreases. We expanded the size of the graphene supercells up to 10×10 , corresponding to a Co coverage down to 1%, and found that the value of Δ_1 remains almost unchanged within this coverage range, as shown in Fig. 2(d). In addition to Δ_1 , there are also two type-I gaps ($\Delta_2 = 8.1$ meV and $\Delta_3 = 3.4$ meV) around $+0.19$ eV and -0.32 eV, respectively, as shown in Fig. 2(c) and 3(a). These gaps stem from the interspin SOC interactions, and they decrease monotonically with the drop of the Co coverage [Fig. 2(d)].

Now we need to see if the SOC induced gaps are non-trivial and give rise to the QAHE [10–12]. The QAHE is characterized by the quantized anomalous Hall conductivity: $\sigma_{xy} = C(e^2/h)$, where C is known as the Chern number [17, 18] and can be calculated from

$$C = \frac{1}{2\pi} \int_{BZ} \Omega(\mathbf{k}) d^2k. \quad (1)$$

The integrand $\Omega(\mathbf{k})$ is the Berry curvature of all occupied states and can be expressed as [18, 30]

$$\Omega(\mathbf{k}) = 2\text{Im} \sum_{n \in \{o\}} \sum_{m \in \{u\}} \frac{\langle \psi_{n\mathbf{k}} | v_x | \psi_{m\mathbf{k}} \rangle \langle \psi_{m\mathbf{k}} | v_y | \psi_{n\mathbf{k}} \rangle}{(\varepsilon_{m\mathbf{k}} - \varepsilon_{n\mathbf{k}})^2}, \quad (2)$$

where $\{o\}$ and $\{u\}$ stand for the occupied and unoccupied states, respectively; $\psi_{n\mathbf{k}}$ and $\varepsilon_{n\mathbf{k}}$ are the spinor Bloch wavefunction and eigenvalue of the n th band at \mathbf{k} point; and $v_{x(y)}$

is the velocity operator. The Berry curvature and Chern number ($C = 2$) of Fe/graphene for perpendicular spin orientation (see Fig. S2) are in good agreement with previous calculation [11], which manifests the validity of our implementation.

The E_F dependent σ_{xy} of Co/graphene is plotted in Fig. 3(b), and it is obvious that σ_{xy} is quantized in all gaps mentioned above. Since the gaps Δ_2 and Δ_3 are opened by the interspin SOC interactions, it is understandable that they have $C = \pm 2$, similar to what was reported for Fe/graphene [11]. One important finding here is $C = 1$ in the gap Δ_1 , even though the majority spin channel is metallic. In fact, we found that the contribution of the majority spin states to the Chern number within Δ_1 is negligible. Therefore, the quantized σ_{xy} within Δ_1 results dominantly from the minority spin states. In other word, Co/graphene behaves like a metal in the majority spin channel, while it is a Chern insulator in the minority spin channel. Accordingly, Co/graphene can be classified as a Chern half metal, in addition to conventional Chern insulators. We may perceive that a Co/graphene nanoribbon has quantized current carrying minority spin along the edges, together with majority spin current in the interior region. This may offer new opportunities for the design of spin filters and spintronics devices.

To reveal the origin of the quantized σ_{xy} in Δ_1 , we plotted the $\Omega(\mathbf{k})$ along the high symmetric direction in the two-dimensional Brillouin zone (2DBZ) in Fig. 3(c). Clearly, there are two dominant peaks around the middle points of $\Gamma\mathbf{K}$ and $\Gamma\mathbf{M}$. From equation (2), $\Omega(\mathbf{k})$ is related to the velocity matrix elements $\langle v_{x(y)} \rangle$ and energy separation between occupied and unoccupied states. By analyzing $\langle v_{x(y)} \rangle$, we found that these peaks result from the coupling between the

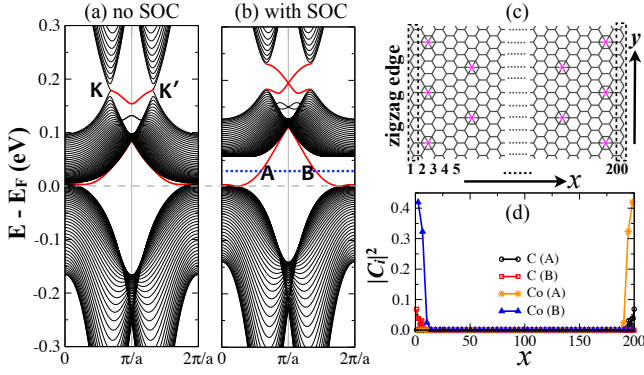


FIG. 4: **Edge states of Co/graphene nanoribbon.** (a) and (b) The band structures of Co/graphene nanoribbon without and with SOC. The gray dashed line indicates the natural E_F and the blue dotted line notated the tuned E_F which locates at the middle point of the band gap. (c) The geometry of the Co/graphene nanoribbon used in our calculation. The width of the nanoribbon is 200 zigzag C chains, and the Co adatoms are distributed uniformly with coverage of 6.25% (same as one Co adatom in 4×4 graphene). The open and periodic directions are notated as \mathbf{x} and \mathbf{y} , respectively. (d) The spatial distributions of the edge states A and B as marked in (b). $|C_i|^2$ is the weights of the zigzag C chains and Co adatoms.

Co $d_{xz/yz}$ orbitals in the minority spin channel, as mentioned above. Considering their hybridizations with the graphene π bands, we can write their wavefunctions as $\psi_{n\mathbf{k}} = C_d^n \phi_d + C_\pi^n \phi_\pi$. The nonzero $\langle \psi_{n\mathbf{k}} | v_x | \psi_{m\mathbf{k}} \rangle$ requires selection rules of $\Delta l = \pm 1$ and $\Delta m = \pm 1$ between $\psi_{n\mathbf{k}}$ and $\psi_{m\mathbf{k}}$. Accordingly, the nonzero $\langle v_{x(y)} \rangle$ comes from the coupling between the Co $d_{xz/yz}$ orbitals and graphene π states. From Fig. 3(c), we can see that the weight of the π states $|C_\pi|^2$ is very small around the Γ point and it increases significantly near the middle points of $\Gamma\mathbf{K}$ and $\Gamma\mathbf{M}$, giving rise to the surge of $\Omega(\mathbf{k})$. On the other hand, the energy separation between these two bands increases rapidly beyond the middle points of $\Gamma\mathbf{K}$ and $\Gamma\mathbf{M}$ as can be seen in Fig. 3(b). This is why $\Omega(\mathbf{k})$ decreases afterwards in Fig. 3(c). More complete information regarding the distribution of the $\Omega(\mathbf{k})$ in the whole 2DBZ is displayed in the upper panel of Fig. 3(d). For comparison, we plotted the distribution of the $\Omega(\mathbf{k})$ of the gap Δ_2 in the lower panel of Fig. 3(d). It can be seen that only a few small vicinities around the K and K' points have contributions to the $\Omega(\mathbf{k})$ of Δ_2 , but their magnitudes are much larger than that of Δ_1 , corresponding to the fact that the interspin SOC interactions are localized within very tiny region where bands cross.

It is known that nonzero integer Chern numbers for the type-I and type-II TI gaps of a infinite 2D system guarantee the quantized edge states when it is cut into one-dimensional ribbons [17]. To check whether similar quantized edge states exist for the type-III gap Δ_1 , we developed a TB model with the Hamiltonian $H = H_g + H_a + H_c$ [20] to directly study the electronic structure of a Co/graphene nanoribbon (NR). Here, H_g , H_a and H_c describe graphene, Co, and the hopping between Co 3d orbitals and graphene π orbitals, respectively. The details about our TB Hamiltonian can be found in sup-

plemental material. The parameters were obtained by fitting the DFT band structures of the 4×4 Co/graphene in Fig. 2(a) and 2(b). The TB band structures (Fig. S5) agree with the DFT band structures very well, which demonstrates the high quality of our approach for the description of Co/graphene.

We used a graphene NR with zigzag edges on both sides to show the existence of the quantized edge states. The width of the graphene NR is 200 zigzag C chains, and the lattice constant along the periodic direction is 4 times of that of graphene. The Co adatoms with a coverage of 6.25% are distributed uniformly on the graphene NR. The corresponding band structures in the minority spin channel without and with the SOC in the one-dimensional Brillouin zone (1DBZ) are plotted in Fig. 4(a) and 4(b). It can be seen that the bands near the E_F remain close without the SOC. When the SOC is considered, these bands are separated by about 54 meV, slightly smaller than the gap Δ_1 (58 meV) of the 2D Co/graphene [Fig. 4(b) and Fig. S5]. Interestingly, we can see that two gap-less bands cross the bulk gap Δ_1 , presumably being from the edges. To prove this, we calculated the weights of all atoms for the wavefunctions of the states A and B marked in Fig. 4(b). The summations over atoms with the same x as marked in Fig. 4(c) are plotted in Fig. 4(d). Strikingly, their wavefunctions indeed localize near the right and left edges, respectively, and the weights decay very rapidly to zero towards the center of the Co/graphene NR. The depth of the edge states is about 22 Å. Note that the edge states do not interact with the majority spin states, as presented in Fig. S6.

When the Fermi level locates in the gap, e.g. at position of the blue dotted line in Fig. 4(b), the edge states contribute to the quantized conductivity. The velocity of conducting electrons can be calculated as $v(\mathbf{k}) = \partial E / \partial \mathbf{k}$. Therefore, the electrons on the right edge (corresponding to the states around A) move along the y direction, while the electrons on the left edge (corresponding to the states around B) move oppositely. Moreover, there's only one conducting channel on each side of the edges, corresponding to the Chern number $C = 1$ obtained by the DFT calculations in 2DBZ. Intriguingly, the edge states are robust upon randomness of the distribution of Co adatoms (see supplemental material), which is the consequence of the weak dependence of the gap Δ_1 on the Co coverage. Therefore, the quantized edge states and hence the QAHE have been demonstrated by both DFT and TB calculations.

To determine the temperature limit for the observation of the QAHE, we need consider a few factors. (i) The MAE of 5.3 meV ensures the perpendicular spin orientation stable up to ~ 60 K. (ii) The TI gap (indirect/direct band gap of 35.7/58 meV) in minority spin channel is larger than the exciton energy at room temperature. (iii) The energy barrier of Co adatom diffusion on graphene is about 0.4 eV [31], which implies that the aggregation of Co adatoms can be avoided below 100 K. Therefore, the temperature limit to observe the QAHE in Co/graphene in experiment mainly depends on the stability of the perpendicular spin orientation, i.e. ~ 60 K which is much higher than that in Cr-doped $(\text{Bi,Sb})_2\text{Te}_3$ [15].

The TI gap and MAE may be further enhanced if we use Rh. We found that the band structures of Rh/graphene (Fig. S4) are very similar with those of Co/graphene, except that the E_F locates ~ 20 meV above the conduction band minimum in the minority spin channel. The indirect (direct) band gap (Δ_1) is 100 (118) meV in minority spin channel near the E_F , and the majority spin channel is metallic with linear bands crossing the E_F . A Chern number $C = 1$ is obtained for the gap Δ_1 , and hence Rh/graphene should have more robust topological features than Co/graphene. Furthermore, the MAE of Rh/graphene is 11.5 meV, which indicates the perpendicular spin orientation to be stable up to ~ 140 K.

In summary, Co/graphene and Rh/graphene are revealed to be excellent Chern half metals, through DFT calculations and TB model analyses. We found that the Co/graphene and Rh/graphene have huge type-III TI gaps (~ 50 and 100 meV) and large perpendicular magnetic anisotropy energies (5.3 and 11.5 meV). Therefore, they are ideal model systems for the observation of the QAHE at elevated temperature. We expect that the TI phase found here may be generalized to other material and may find significant applications in quantum computing and spintronics devices.

Acknowledgments

J.H. and Z.Z. thank useful discussions with Jason Alicea and Xiaoliang Qi. This work was supported by DOE-BES Grant No. DE-FG02-05ER46237 and by NERSC for computing time (J.H. and R.W.), NSF Grant No. DMR-1161348 (Z.Z.).

* Corresponding author: wur@uci.edu

- [1] C. L. Kane and E. J. Mele, Phys. Rev. Lett. **95**, 226801 (2005).
- [2] B. A. Bernevig, T. L. Hughes, and S.-C. Zhang, Science **314**, 1757 (2006).
- [3] M. König, S. Wiedmann, C. Brune, A. Roth, H. Buhmann, L. W. Molenkamp, X.-L. Qi, and S.-C. Zhang, Science **318**, 766 (2007).
- [4] Y. Xia, D. Qian, D. Hsieh, L. Wray, A. P. d H. Lin, A. Bansil, D. Grauer, Y. S. Hor, R. J. Cava, and M. Z. Hasan, Nat. Phys. **5**, 398 (2009).
- [5] H. J. Zhang, C.-X. Liu, X.-L. Qi, X. Dai, Z. Fang, and S.-C. Zhang, Nat. Phys. **5**, 438 (2009).
- [6] M. Z. Hasan and C. L. Kane, Rev. Mod. Phys. **82**, 3045 (2010).
- [7] X.-L. Qi and S.-C. Zhang, Rev. Mod. Phys. **83**, 1057 (2011).
- [8] N. Nagaosa, Science **318**, 758 (2007).
- [9] C.-X. Liu, X.-L. Qi, X. Dai, Z. Fang, and S.-C. Zhang, Phys. Rev. Lett. **101**, 146802 (2008).
- [10] R. Yu, W. Zhang, H.-J. Zhang, S.-C. Zhang, X. Dai, and Z. Fang, Science **329**, 61 (2010).
- [11] Z. Qiao, S. A. Yang, W. Feng, W.-K. Tse, J. Ding, Y. Yao, J. Wang, and Q. Niu, Phys. Rev. B **82**, 161414 (2010).
- [12] H. Zhang, C. Lazo, S. Blügel, S. Heinze, and Y. Mokrousov, Phys. Rev. Lett. **108**, 056802 (2012).
- [13] K. F. Garrity and D. Vanderbilt, Phys. Rev. Lett. **110**, 116802 (2013).
- [14] E. H. Hall, Philos. Mag. **12**, 157 (1881).
- [15] C.-Z. Chang, J. Zhang, X. Feng, J. Shen, Z. Zhang, M. Guo, K. Li, Y. Ou, P. Wei, L.-L. Wang, et al., Science **340**, 167 (2010).
- [16] Z. F. Wang, Z. Liu, and F. Liu, Phys. Rev. Lett. **110**, 196801 (2013).
- [17] Y. Hatsugai, Phys. Rev. Lett. **71**, 3697 (1993).
- [18] D. J. Thouless, M. Kohmoto, M. P. Nightingale, and M. den Nijs, Phys. Rev. Lett. **49**, 405 (1982).
- [19] C. Weeks, J. Hu, J. Alicea, M. Franz, and R. Wu, Phys. Rev. X **1**, 021001 (2011).
- [20] J. Hu, J. Alicea, R. Wu, and M. Franz, Phys. Rev. Lett. **109**, 266801 (2012).
- [21] J. Ding, Z. Qiao, W. Feng, Y. Yao, and Q. Niu, Phys. Rev. B **84**, 195444 (2011).
- [22] X. Wang, R. Wu, D.-S. Wang, and A. J. Freeman, Phys. Rev. B **54**, 61 (1996).
- [23] R. Wu and A. J. Freeman, J. Magn. Magn. Mater. **200**, 498 (1999).
- [24] J. Hu and R. Wu, Phys. Rev. Lett. **110**, 097202 (2013).
- [25] T. Eelbo, M. Waśniowska, P. Thakur, M. Gyamfi, B. Sachs, T. O. Wehling, S. Forti, U. Starke, C. Tieg, A. I. Lichtenstein, et al., Phys. Rev. Lett. **110**, 136804 (2013).
- [26] F. Donati, Q. Dubout, G. Autès, F. Patthey, F. Calleja, P. Gambardella, O. V. Yazyev, and H. Brune, Phys. Rev. Lett. **111**, 236801 (2013).
- [27] Y. Virgus, W. Purwanto, H. Krakauer, and S. Zhang, Phys. Rev. B **86**, 241406 (2012).
- [28] D.-S. Wang, R. Wu, and A. J. Freeman, Phys. Rev. B **47**, 14932 (1993).
- [29] J. Hu and R. Wu, arXiv:1305.5978 (2013).
- [30] Y. Yao, L. Kleinman, A. H. MacDonald, J. Sinova, T. Jungwirth, D.-S. Wang, E. Wang, and Q. Niu, Phys. Rev. Lett. **92**, 037204 (2004).
- [31] O. V. Yazyev and A. Pasquarello, Phys. Rev. B **82**, 045407 (2010).